Paleomagnetism indicates that primary magnetite in zircon records a strong Hadean geodynamo

John A. Tarduno[a,b,1], Rory D. Cottrell[a], Richard K. Bono[a,2], Hirokuni Oda[c], William J. Davis[d], Mostafa Fayek[e], Olaf van 't Erve[f], Francis Nimmo[g], Wentao Huang[a], Eric R. Thern[h,i], Sebastian Fearn[j], Gautam Mitra[a], Aleksey V. Smirnov[k], and Eric G. Blackman[b]

[a]Department of Earth and Environmental Sciences, University of Rochester, Rochester, NY 14627; [b]Department of Physics and Astronomy, University of Rochester, Rochester, NY 14627; [c]Research Institute of Geology and Geoinformation, Geological Survey of Japan, National Institute of Advanced Industrial Science and Technology (AIST), Tsukuba 305-8567, Japan; [d]Geological Survey of Canada, GSC-Central Canada, Geochronology, Ottawa, ON K1A 0E8, Canada; [e]Department of Geological Sciences, University of Manitoba, Winnipeg, MB R3T 2N2, Canada; [f]Materials Science and Technology Division, Naval Research Laboratory, Washington, DC 20375; [g]Department of Earth and Planetary Sciences, University of California, Santa Cruz, CA 95064; [h]Geochron Research Group, Bentley, WA 6982, Australia; [i]Department of Applied Physics, Curtin University of Technology, Perth, WA 6001, Australia; [j]Department of Geoscience, University of Wisconsin–Milwaukee, Milwaukee, WI 53201-0413; and [k]Department of Geological and Mining Engineering and Sciences, Michigan Technological University, Houghton, MI 49931

Edited by Lisa Tauxe, University of California San Diego, La Jolla, CA, and approved December 12, 2019 (received for review September 24, 2019)

Determining the age of the geomagnetic field is of paramount importance for understanding the evolution of the planet because the field shields the atmosphere from erosion by the solar wind. The absence or presence of the geomagnetic field also provides a unique gauge of early core conditions. Evidence for a geomagnetic field 4.2 billion-year (Gy) old, just a few hundred million years after the lunar-forming giant impact, has come from paleomagnetic analyses of zircons of the Jack Hills (Western Australia). Herein, we provide new paleomagnetic and electron microscope analyses that attest to the presence of a primary magnetic remanence carried by magnetite in these zircons and new geochemical data indicating that select Hadean zircons have escaped magnetic resetting since their formation. New paleointensity and Pb-Pb radiometric age data from additional zircons meeting robust selection criteria provide further evidence for the fidelity of the magnetic record and suggest a period of high geomagnetic field strength at 4.1 to 4.0 billion years ago (Ga) that may represent efficient convection related to chemical precipitation in Earth's Hadean liquid iron core.

Hadean geodynamo | paleointensity | early Earth conditions

Earth's ancient magnetic field is of fundamental importance because of the role the field plays in protecting the planet's atmosphere and water from removal by the solar wind (1). Hence, the magnetic field is central to the establishment and maintenance of terrestrial planetary habitability (2). Records of the geodynamo also provide a means of probing past core conditions, and thus they can inform us about the thermal evolution of the planet (3, 4). The oldest record of field strength from extant rocks comes from single-crystal paleointensity (SCP) analyses of 3.4 to 3.45-Gy-old (Paleoarchean) dacites of South Africa (5). The presence of the geomagnetic field at these times is also supported by studies of magnetic directions (6, 7). Efforts to recover paleointensity records in even older rocks have been thwarted by ubiquitous metamorphism which has either thermally reset magnetizations or caused chemical transformations that obscure primary magnetic minerals (8). An alternative means to explore the pre-Paleoarchean field is to examine minerals in younger sedimentary rocks that might have escaped metamorphism and chemical change (2). This approach also employs SCP analyses, where crystals carrying magnetic inclusions are interrogated for their net magnetic signature (9). It is crucial that a silicate crystal-sized specimen containing many magnetic inclusions be measured because of the statistical limits imposed by thermodynamics. Maxwell–Boltzmann statistics (10) and classical considerations of relaxation time (11, 12) indicate that only an assemblage of magnetic grains with single domain-like behavior can be expected to record and preserve a primary magnetization on the billion-year timescales needed to explore the most ancient geodynamo. Here we use "single-domain–like" in a phenomenological sense, including single-vortex pseudo–single-domain grains which can also have relaxation times greater than 1 Gy (13). Zircons are attractive targets for SCP analyses to recover the most ancient geomagnetic record because of their durability and because they can be accurately dated using U-Pb geochronology. However, the expansion of the crystal lattice accompanying uranium to lead radioactive decay can create crack pathways for the introduction of fluids. Thus, vigorous protocols must be followed to examine the importance of secondary oxides for the measured net natural remanent magnetization and to exclude zircons which have been compromised by metamictization (1).

Significance

The age and early history of Earth's geomagnetic field can provide insight into the evolution of the core and atmosphere. But measurement of Hadean zircons—the oldest known terrestrial materials—and the determination of the antiquity of their magnetizations are amongst the most challenging endeavors in paleomagnetism. New paleomagnetic, electron microscope, geochemical, and paleointensity data indicate the presence of primary magnetite inclusions in select zircons. These data support the presence of the geomagnetic field, and associated shielding of the atmosphere from the solar wind, ∼4.2 billion years ago. A relatively strong field recorded by these zircons at ∼4 billion years ago may be a signal that chemical precipitation in the core was powering the geodynamo.

Author contributions: J.A.T. designed research; J.A.T., R.D.C., R.K.B., H.O., W.J.D., M.F., O.v.'t.E., W.H., E.R.T., and S.F. performed research; J.A.T., R.D.C., R.K.B., H.O., W.J.D., O.v.'t.E., F.N., G.M., A.V.S., and E.G.B. analyzed data; J.A.T. wrote the paper with contributions from the coauthors; J.A.T., R.K.B., E.R.T., and S.F. performed field studies; J.A.T., F.N. and E.G.B. performed geodynamic interpretations; G.M. provided microstructural interpretation; and A.V.S. provided rock magnetic interpretation.

The authors declare no competing interest.

This article is a PNAS Direct Submission.

Data deposition: Magnetic datasets generated during and/or analyzed in this study have been deposited in the MagIC repository, http://earthref.org/MagIC/16680.

[1]To whom correspondence may be addressed. Email: john.tarduno@rochester.edu.

[2]Present address: Geomagnetism Laboratory, University of Liverpool, Liverpool L69 3GP, United Kingdom.

This article contains supporting information online at https://www.pnas.org/lookup/suppl/doi:10.1073/pnas.1916553117/-/DCSupplemental.

First published January 21, 2020.

Tarduno et al. (1) reported the first paleointensity measurements of zircons, which were collected from the Discovery outcrop (14) of the Jack Hills of Western Australia (*SI Appendix*, Fig. S1). After robust selection criteria, less than 2% of the zircons isolated were suitable for paleointensity recording. These select zircons yielded a paleointensity history starting at 3.2 Ga, with values similar to those recorded by SCP analyses from extant rocks (15), to more variable intensities ranging as old as 4.2 Ga. The latter values extend the record of the geodynamo by more than 750 million years (My) into the Hadean Eon, just a few hundred million years after the giant impact that formed the Moon (16).

Closely following the Tarduno et al. (1) study, paleointensities from ∼5-My-old zircons that agreed with global data were reported (17), further supporting the fidelity of this crystal type as a paleomagnetic recorder. However, in light of the importance of evidence for a Hadean geodynamo, there has also been an intense effort to disprove the results. Herein, we address these critiques and further our definition of the earliest geodynamo. We first return to the basic test used to explore the impact of secondary magnetizations in Jack Hills zircons, the microconglomerate test. We expand this test to define the secondary magnetization direction that is recorded by the Jack Hills zircons at low unblocking temperatures and show how this differs from the magnetization used to define the Eoarchean to Hadean geodynamo. We show how the microconglomerate test results, and considerations of statistical requirements for recording the field, are inconsistent with the interpretation that secondary magnetic particles carry an important natural remanent magnetization signal. Instead, microconglomerate tests further support the presence of a magnetization carried by magnetite in zircons that predates deposition. These results, together with new optical (reflected light) microscopy, scanning electron microscopy (SEM), focused ion beam (FIB) analyses, magneto-optical Kerr effect (MOKE) measurements, and transmission electron microscope (TEM) analyses, indicate the presence of primary magnetite inclusions in Jack Hills zircons. We show how new Pb and Li analyses support the interpretation that select Hadean Jack Hills zircons have not seen thermal processing between their formation and incorporation into the conglomerate that would have reset their primary high-temperature magnetizations. Zircons compromised by metamictization/alteration studied by others are not representative of those used in our SCP analyses. We present new paleomagnetic, paleointensity, and Pb-Pb radiometric age data on zircons meeting selection criteria (1) that provide further evidence for continuity of the geodynamo and attendant magnetic shielding of the terrestrial atmosphere since Hadean times. Finally, the new data provide emerging evidence for a period of high fields near 4.0 to 4.1 Ga which imply a vigorously convecting Hadean core that may be driven by effects in addition to purely thermal buoyancy (e.g., chemical precipitation).

Magnetic Overprint at the Jack Hills Discovery Site

The Jack Hills have been affected by greenschist grade metamorphism that reached peak temperatures of approximately 420 to 475 °C at an age of 2,655 ± 5 million-years ago (Ma) (18, 19); this event corresponds with Pb loss at ∼2.65 Ga, the most significant postdeposition event seen in zircons analyzed by Tarduno et al. (1) from the Discovery Site. To test whether the zircons isolated from the microconglomerate were magnetically reset by the metamorphism, Tarduno et al. (1) conducted a microconglomerate test. Thin sections ∼300 to 500 μm thick were cut from the conglomerate and individual zircons (150 to 250 μm in size) surrounded by clean quartz (for a total size of 500 to 800 μm diameter), oriented relative to the slide, were isolated. These measurements, and those of single zircons, are among the most challenging in paleomagnetism because of the low natural remanent magnetization (NRM) moments, often $<1 \times 10^{-12}$ A m^2. These specimens were demagnetized with a CO_2 laser (15), which has the important advantage of heating over very short time intervals (e.g., 90 s) compared to paleomagnetic ovens (generally $\gg 20\times$ longer), greatly reducing the possibility of laboratory-induced alteration, an issue crucial for reliable paleointensity determination (9). The magnetization isolated at high unblocking temperatures from the specimens (in this case >550 °C to 580 °C and indicative of a magnetite carrier) passed a test for randomness (20), excluding scenarios for remagnetization after deposition of the Jack Hills conglomerate at ∼3 Ga (18). As we will discuss, these data are also inconsistent with the characteristic magnetizations being secondary and acquired after zircon formation but prior to deposition.

While the zircon specimens were oriented with respect to each other in the Tarduno et al. (1) study, the rock from which they were cut was not geographically oriented. Therefore, there was no means of comparing the paleomagnetic directions from the zircons with any global magnetization that might have been imparted during peak metamorphism. Furthermore, the magnetization direction at the time of peak metamorphism at the Discovery Site was unknown. Subsequently, a constraint on the magnetization associated with metamorphism was derived by Cottrell et al. (21) who studied the metamorphic chromemica fuchsite [$K(Al,Cr)_2(AlSi_3O_{10})(OH)_2$]. Oriented fuchsite grains were isolated from a field-oriented sample adjacent to the one yielding zircons from the Tarduno et al. (1) study. The magnetic carriers in the fuchsite are relict Fe-Cr grains (21) clearly imaged in SEM analyses with compositions constrained by energy-dispersive X-ray spectroscopy (EDS). We note that a critique claiming that the magnetic carrier in the fuchsite is pyrrhotite (22) is erroneous: Unblocking temperatures exceed the sharp 320 °C Curie temperature of terrestrial pyrrhotite (12) and EDS data sufficient for the identification of pyrrhotite [$Fe_{1-x}S$ (x = 0 to 0.17)] (23) show that there is no sulfur in the Fe-Cr particles (21). Fuchsite specimens yielded coherent magnetizations at unblocking temperatures between ∼270 and 340 °C that allow for the rejection of the conglomerate test's null hypothesis of randomly oriented magnetizations (20, 21). Because the magnetizations come from a secondary (metamorphic) mineral phase, this constitutes a positive inverse conglomerate test useful for further gauging overprint directions carried by the zircons. Bono et al. (24) found that the fuchsite magnetization passed a fold test at the 90% confidence level with an overprint magnetization isolated in cobble-sized conglomerates ∼1 km from the Discovery Site (25). Bono et al. (24) also isolated this magnetization in data from a study claiming that the Jack Hills were affected by a "pervasive" 1-Ga remagnetization (26). This issue is important because pervasive late thermochemical and/or thermoviscous remagnetizations are well known in younger terrains (12); if the Jack Hills had been similarly affected, their zircons would not be expected to preserve primary magnetizations and there would be no point in pursuing measurements of their natural remanent magnetizations. However, the analyses of Cottrell et al. (21) and Bono et al. (24) conclusively demonstrate that the claim of a pervasive 1-Ga magnetization in the Jack Hills is incorrect. Moreover, a 1-Ga direction has not been reproduced after resampling of Jack Hills monzogranites (27). In data from sediments near the Discovery Site, the reported 1-Ga direction (26) has been shown to be artifactual (28, 29).

Rather than a late remagnetization, the magnetic data from the Jack Hills support a straightforward interpretation consistent with local and regional geology: A low to intermediate unblocking temperature magnetic overprint was acquired during peak metamorphism at 2,655 ± 5 Ma (18, 19) coincident with, and likely caused by, intrusion of the Jack Hills monzogranites dated at 2,654 ± 7 Ma (30) (*SI Appendix*, Fig. S1). With the foundation of the true overprint magnetization at the Jack Hills

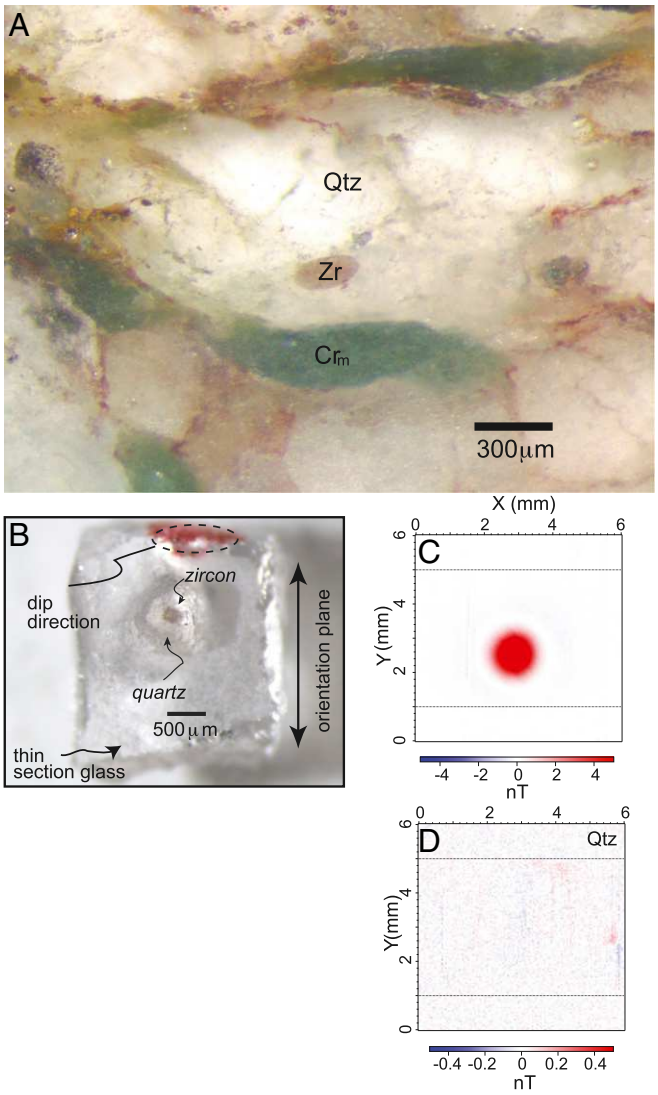

Fig. 1. Jack Hills Discovery Site zircon magnetization. (*A*) Photomicrograph of 300-μm-thick thin section used to isolate samples for microconglomerate test. Cr_m, chrome–mica fuchsite; Qtz, quartz; Zr, zircon. (*B*) Specimen of zircon and surrounding quartz extracted from thin section and used for paleomagnetic measurement with orientation information (*Materials and Methods*). (*C*) AIST SSM measurement of zircon and quartz after application of a pTRM at 575 °C in a 61-μT applied field. (*D*) AIST SSM measurement of quartz only after application of a pTRM at 575 °C in a 61-μT applied field. Note order-of-magnitude change in scale relative to *C*.

Discovery Site established, we now address the limitations of the original microconglomerate test (1) by new analyses of an adjacent host rock oriented in the field.

An Improved Microconglomerate Test

Procedures for the microconglomerate test follow those of Tarduno et al. (1) with the exception that additional thermal demagnetization steps were added to better assess the low unblocking temperature magnetization. Analyses were carried out in the University of Rochester three-layer magnetically shielded room (field <200 nT) using the ultrahigh-sensitivity direct-current superconducting quantum interference device (SQUID) magnetometer (William S. Goree, Inc.). Before proceeding to an analysis of the directions, we address a criticism claiming that the magnetizations of the initial Discovery Site microconglomerate test are carried by the material surrounding the zircons (31), which is microcrystalline quartz selected such that it lacks opaque minerals (1), rather than the zircon itself. We used one of the specimens from the Tarduno et al. (1) study (Fig. 1*A*) and mounted it in a glass slide (Fig. 1*B*) screened to have a negligible magnetic remanence. A partial thermoremanent magnetization (pTRM) at 575 °C was applied using a CO_2 laser in the presence of a 61-μT field at AIST Japan and subsequently measured with the AIST scanning SQUID magnetometer (SSM) (32) (*Materials and Methods*). A clear magnetic signature is observed (Fig. 1*C*). Next, quartz adjacent to where the zircon specimen was obtained was mounted on a glass slide, and an identical pTRM (i.e., 575 °C, 61-μT field) was applied. No significant magnetization can be seen in the region of the quartz or on the slide (any minor magnetization signals are nonrepeatable and attributable to the plastic cover used for the SQUID microscope measurements) (Fig. 1*D*). These data thus disprove the critique (31) and verify the cleanliness of the mounting materials used in the Tarduno et al. (1) study and in the work described below.

Demagnetization of new zircons-in-quartz specimens yields a clear high-unblocking temperature component of magnetization and one or more components at lower unblocking temperatures (Fig. 2 *A* and *B* and *SI Appendix*, Fig. S2). The high-temperature

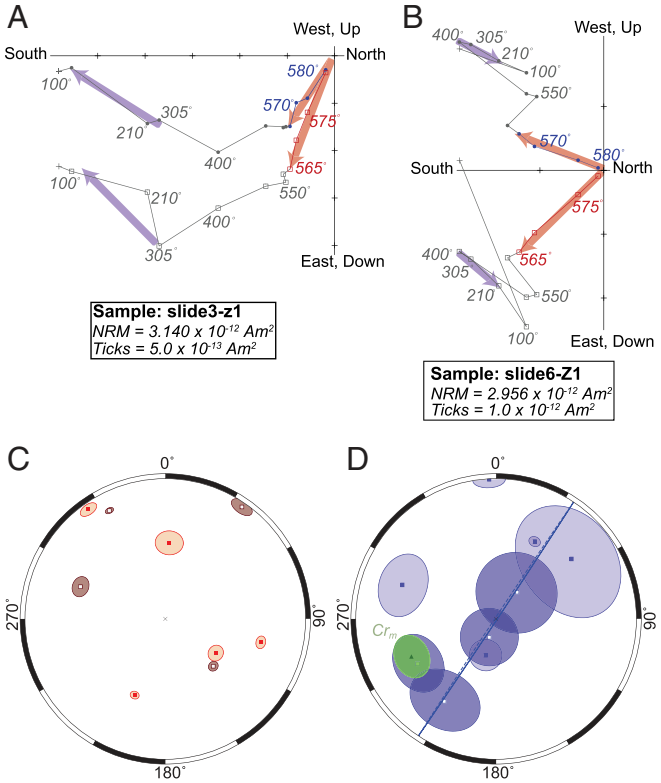

Fig. 2. Jack Hills microconglomerate test. (*A* and *B*) Example orthogonal vector plot of thermal demagnetization of microconglomerate specimens. Temperatures labeled are °C. Horizontal projection of the magnetization (declination) is shown with solid circles; vertical projection (inclination) is shown with open squares. Red arrows, high unblocking (characteristic) remanent magnetization. Purple arrows, low unblocking/intermediate temperature magnetization. (*C*) Equal area stereonet projection of high unblocking characteristic magnetizations. Uncertainties are maximum angular deviation values of principal component fits. Solid symbols, lower hemisphere (positive inclination); open symbols, upper hemisphere (negative inclination). (*D*) Equal area stereonet projection of low/intermediate unblocking magnetizations together with direction from the chrome–mica fuchsite (triangle, Cr_m) from Cottrell et al. (21). Conventions are as in *C*. Also shown is great circle fit (solid/dashed line) to low/intermediate unblocking magnetizations.

component (isolated between 565 and 580 °C) passes a statistical test for randomness (i.e., the null hypothesis cannot be rejected at the 5% significance level; *SI Appendix*, Table S1 and Fig. 2*C*). The high-unblocking temperature data correspond with a uniform (random) distribution with positive support in the Bayesian approach of Heslop and Roberts (33), whereas no viable data clusters that might indicate partial magnetic overprinting are seen using the approach of Bono et al. (24) which searches for clusters in data that might represent partial magnetic overprinting (*SI Appendix*).

While there is no evidence for a remagnetization in the high-unblocking temperature magnetizations using these three tests, there is, arguably, a nuanced incompleteness. Because the zircons have seen low-grade metamorphism at ∼2.65 Ga, they should retain some vestige of this magnetization if the zircons contain a range of magnetic inclusion sizes, including larger particles with lower unblocking temperatures and relaxation times. To examine this issue, we now turn our attention to the low unblocking temperature magnetizations. A central challenge in this analysis is that for a distribution of magnetic carriers with dominantly single-domain–like behavior, the number of grains reset and carrying the secondary magnetization is expected to be small. Nevertheless, a coarse low-temperature component is seen in the same nine samples (typically isolated between 100 and 400 °C) (Fig. 2*D* and *SI Appendix*, Table S1).

Interestingly, the three approaches to the conglomerate tests again suggest that a random distribution cannot be excluded (*SI Appendix*). However, visual inspection reveals that the low-temperature components clearly differ in their distribution from the high-unblocking component. The former trend along a great circle between the magnetization directions from fuchsite (21) and the low- and intermediate-temperature component mode A isolated from cobble remanences (24) and its antipode (Fig. 2*D*). This reveals a limitation of the aforementioned approaches to the conglomerate test: Their probative power is in comparing unimodal and uniform distributed data. Other distributions of geomagnetic and geologic significance, such as a great circle distribution between two polarities, could appear to be uniformly distributed without additional inspection of the data. The observed distribution suggests that the low unblocking temperature component recorded by the zircons was acquired while the geomagnetic field was reversing during peak metamorphism of the Jack Hills. Hence, the presence of the expected overprint and its difference from the high unblocking temperature characteristic remanence are foundational observations defining the fidelity of the Jack Hills (JH) zircons as magnetic records. With this context, we next discuss the nature of the magnetic carriers in the zircons at multiple scales.

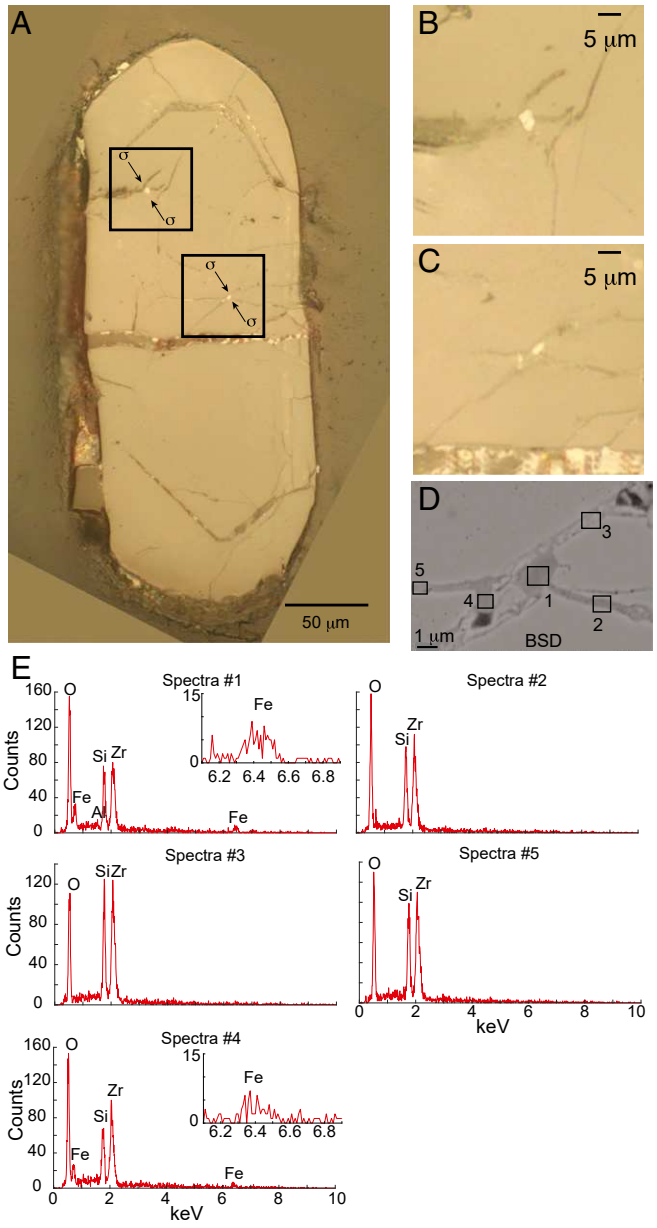

Fig. 3. Optical (reflected light) and SEM analyses of large (1 to 3 μm) magnetite inclusions in JH zircon. (*A*) Reflected light image (zircon RZ64). (*B* and *C*) Partially oxidized magnetite inclusions in crack. Other bright areas (at base) are other reflectors (i.e., not Fe). (*D* and *E*) SEM backscatter detector (BSD) image (*D*) of region *C* with EDS analysis spots (1–5) and corresponding spectra (*E*). Also shown is possible stress orientation (σ) in *A*, suggesting cracks emanating from inclusion in *B* and *C* were formed under the influence of the same stress field.

Evidence for Primary JH Magnetic Inclusions

We recall that Tarduno et al. (1) noted that "Sources of magnetite within the JH zircons include isolated inclusions trapped in the zircon matrix, vapor phase magnetite associated with voids, and magnetite inclusions within other silicates trapped in the zircons" (ref. 1, p. 4, *SI Appendix*). Preliminary data bearing on these occurrences were presented by Bono et al. (34) and Tarduno et al. (35) and are expanded upon here. We examined 95 JH zircons using reflected light and SEM analyses (*Materials and Methods*). We start with a consideration of relatively large (∼1 to 3 μm) iron oxide inclusions that are seen in about 10% of the zircons (Fig. 3). This is an underestimate of the percentage of zircons with such inclusions because each of these analyses examined only a single cut through a given crystal, with a viewing area $<<1\%$ of the total zircon volume. Inclusions of this size are found throughout the zircons and are not restricted to edges (cf. ref. 31). Some of these particles are probably in the multidomain (MD) state; they are not principal contributors to the high unblocking temperature magnetization used to constrain paleointensity because these analyses employ MD tests (1). However, these inclusions can contribute to the low unblocking temperature magnetization (Fig. 2) and they are most likely the largest representatives of a grain size distribution that extends down to sizes including pseudo–single-domain (PSD) and single-domain (SD) particles. The large inclusions observed are commonly found along cracks. While most of the zircons examined would not be used for paleointensity analyses because of the rigorous selection criteria (1) that exclude physically altered crystals, the relationship between cracks and inclusions provides critical insight into the primacy of Jack Hills zircon magnetic inclusions. Specifically, magnetite inclusions, so

identified by their reflected light character (*SI Appendix*), occur at the intersection of cracks that cut across internal zircon oscillatory zoning (Fig. 3 and *SI Appendix*, Fig. S3). EDS Fe signals are absent in the cracks; this is inconsistent with secondary formation of inclusions by Fe-enriched fluids. Moreover, the pattern is indicative of crack formation seen at a variety of scales in natural materials that have experienced stress (36, 37). Plastic deformation (38) by dislocation glide within a crystal under stress can be obstructed by inclusions, causing dislocation pile-ups (39), stress concentration, and cracking. This type of crack initiation has been documented in the study of opaque inclusions in quartz from rocks deformed under greenschist grade metamorphic conditions (36). Cracks in JH zircons associated with inclusions most likely formed during the metamorphism and deformation that created the stretched-pebble morphology of the host conglomerate. Thus, critiques based on the assumption that JH inclusions are secondary because some are in cracks (31) are erroneous; the cogent indicators of past processes (i.e., strains leading to stress concentrations) were missed (*SI Appendix*). However, as expected, cracks and crystal disruption associated by metamictization appear to promote inclusion oxidation (*SI Appendix*, Fig. S3), further highlighting the need to apply robust selection criteria (1). Occasionally large magnetite inclusions are found separate from cracks, with the nearest cracks lacking EDS Fe signatures (Fig. 4 *A*–*E* and *SI Appendix*). A few submicrometer-sized particles, as small as ∼200 to 300 nm, were also detected by SEM surveys (e.g., *SI Appendix*, Fig. S4), consistent with our inferences about a grain size distribution of magnetic particles. The small particles detected are in the pseudo–single-domain size range capable of recording the high unblocking temperature remanence (Fig. 4*F*).

Because of the presence of micrometer and submicrometer primary magnetic inclusions, even smaller inclusions within the single-vortex and single-domain size range should be present, as predicted by paleomagnetic analyses (1). Magnetic particles within this size range have been identified in a TEM study of three JH zircons (40) which also reproduced the magnetite-like high-unblocking characteristics. Although none of these zircons would pass our selection criteria (1) and the identification of these small particles as magnetite in nearly all cases still relies on magnetic unblocking temperature data, the results to first order confirm predictions of the Tarduno et al. (1) study. Instead, the authors of ref. 40 attributed these small particles to hypothetical secondary formation processes, calling upon the presence of adjacent dislocations or inclusion elongation as evidence. In contrast, dislocation occurrence adjacent to primary inclusions within a crystal that has experienced stress is expected and not evidence of secondary magnetite (*SI Appendix*). Iron is known to occur in pristine (type-C) zircons (41), as do other nonformula trace elements (e.g., Mn, K, Li). Similar to exsolution in other silicates (3, 9, 42), Fe migration at high temperature could have formed particles elongated along the crystallographic planes with or without the involvement of coprecipitated zircon. We note that elongated particles in ref. 40 resemble vapor-phase Fe that could have formed during initial zircon formation (*SI Appendix*) (43, 44). Yet another argument posited for secondary magnetic particle formation (40) is the occurrence of voids. We note that in most cases the Fe mineral highlighted in ref. 40 cannot be important because its size/volume is below the SD size threshold and that the absence of Fe in the pathways for migration, in our study, is highly problematic for this mechanism (*SI Appendix*). However, we challenge the larger assumption that magnetite inclusion occurrence with void space equates with a secondary formation through analyses below.

We start by noting that with successive polishing, many inclusions in JH zircons appear to be part of multicrystalline aggregates, possibly together with void space. However, disruption through polishing (i.e., inclusion removal) limits interpretation and further exploration of these particles. To avoid surface disruption, we searched for subsurface magnetic structures using MOKE (using NanoMOKE3; *Materials and Methods*) whereby the plane of polarization of an incoming wave is rotated after interaction with a magnetic mineral (45). A well-known limitation of the MOKE technique is the need for a smooth polished surface, which we achieve through colloidal Si polishing (*Materials and Methods*). Some areas of grain roughness are often unavoidable. However, we found a large signal corresponding to an area lacking any surface expression in reflected light (Fig. 5 *A*–*C*). Next, we explored this region with a FIB lift-out (*Materials and Methods*). This revealed a pristine and multicompositional structure at a depth of ∼2 μm (Fig. 5 *D* and *E*). EDS data indicate quartz and feldspars (Fig. 5 *F*–*H*). Iron was detected in one of the feldspars, suggesting it contains magnetic inclusions, as is commonly observed in this silicate type (9, 42). Importantly, void space surrounding the inclusions is clearly primary; the surrounding zircon lacks cracks. Thus, silicate inclusions which are hosts to primary magnetic inclusions can contribute to the magnetic signal of JH zircons (1). FIB trenching confirms that many inclusions are multiphase, and voids are common. We interpret these as primary melt inclusions; vapor-phase magnetite can be one of the included phases. Furthermore, successive polishing shows that these melt inclusions are common in JH zircons; successive polishing also reveals micrometer-sized magnetite inclusions in zircons where they were absent in initial cuts (*SI Appendix*, Figs. S5 and S6).

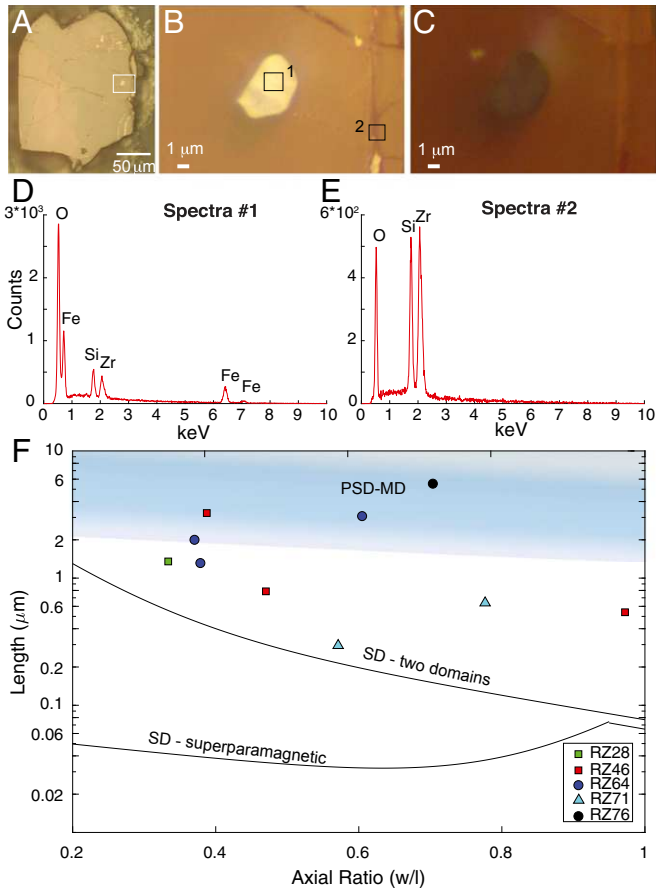

Fig. 4. Reflected light, SEM EDS, and size of iron inclusions in JH zircons. (*A*) Reflected light image with inclusion separate from cracks highlighted (box). (*B* and *C*) Reflected light image (1,000× oil immersion) with 0° (*B*) and 90° (*C*) polarization. Boxes in *B* highlight areas of EDS analysis (*D* and *E*). (*F*) Summary of particles visible identified in reflected light analyses.

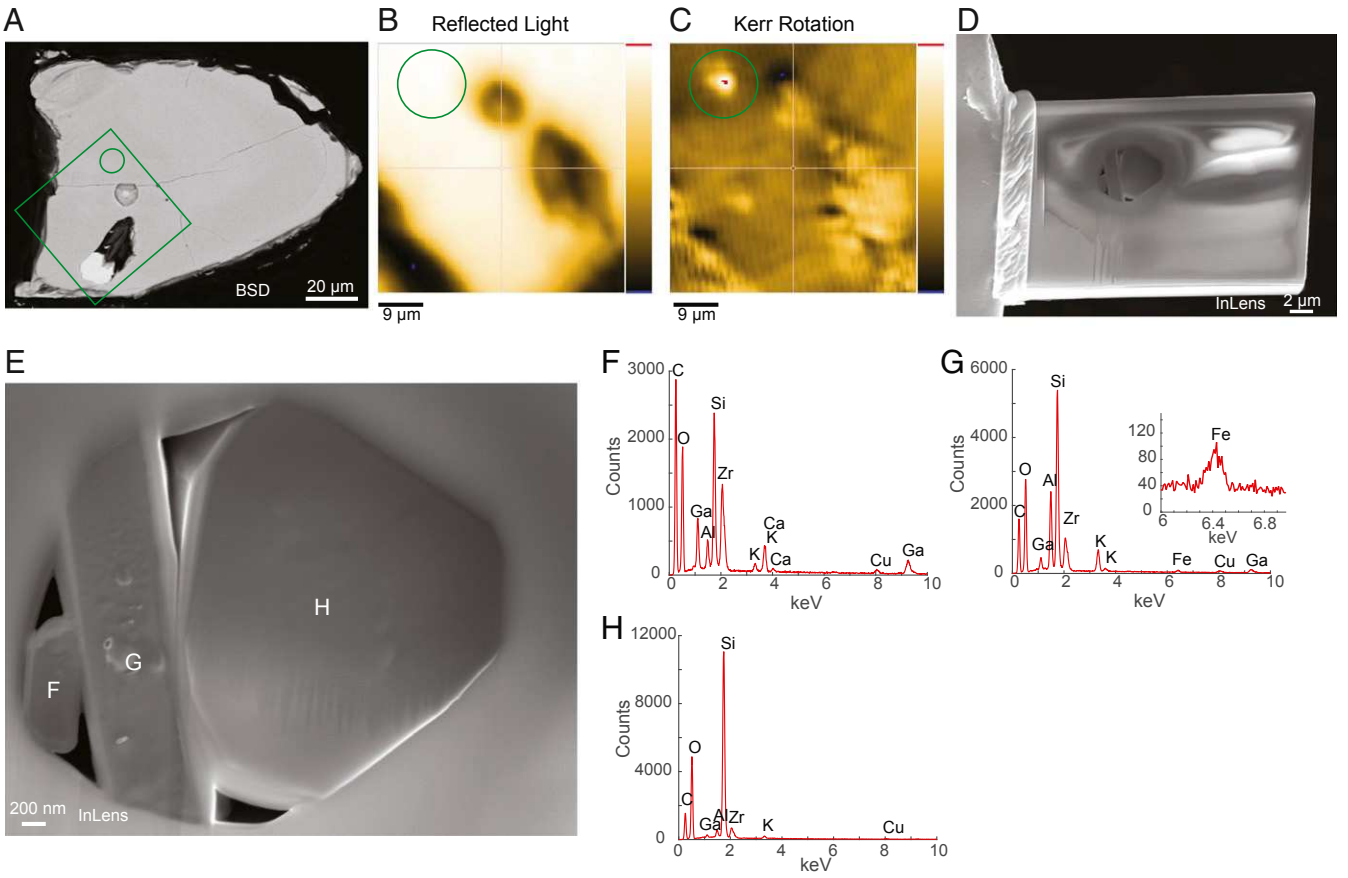

Fig. 5. Primary iron-bearing Jack Hills inclusions. (*A*) SEM image (backscatter detector [BSD] at 20 keV) of zircon. (*B*) NanoMOKE reflected-light image of zircon surface. Green circle highlights area of interest (see *C*). (*C*) NanoMOKE parallel image showing strong Kerr angle response (red inside green reference circle, note scale on right) from area without any surface features (compare with *B*). (*D* and *E*) SEM images (InLens, 20 keV) of focused ion beam lift-out of area (*C*) showing strong NanoMOKE response reveal a buried multicomponent silicate inclusion and voids. (*F–H*) Energy-dispersive analysis reveals the presence of quartz (*H*) and two different compositions of feldspars (*F* and *G*). One of the feldspars (*G*) bears iron that is a likely source of the magnetic signal. Cu and Ga peaks are related to TEM grid and FIB analyses, respectively.

Overall, the lack of a high unblocking temperature overprint, the physics of chemical remanent magnetization (CRM) acquisition, and Maxwell–Boltzmann statistical limits on magnetic recording are a priori inconsistencies with hypothetical models (cf. ref. 40) invoking secondary magnetite as an important remanence carrier in JH zircons (*SI Appendix*). In addition, reported observations on zircons compromised by metamictization/alteration (31, 40) are inappropriate representations of zircons selected for SCP analyses (*SI Appendix*), and magnetizations measured using high fields (31) are artificial and inappropriate representations of the relevant high unblocking temperature magnetization (*SI Appendix*). But even if secondary magnetite formed in some JH zircons, a critique claiming that this "precludes analysis of the Hadean dynamo" (ref. 40, p. 407) is mistaken because it misses the relevant question: presence or absence of the most ancient geodynamo (1). To indicate presence of a core geomagnetic field, paleointensity values must be above a threshold set by an external field induced by the solar wind interacting with a hypothetical Earth without an internal core dynamo (1, 2). Because of the nature of a hypothetical secondary CRM (*SI Appendix*), any bias will be conservative, toward the inability of paleointensity data to distinguish between internal and external fields. We will revisit this issue later with a new dataset. But first we further investigate methods to constrain postformation temperature exposure of JH zircons.

Lithium Diffusion in Magnetized Hadean Zircons

To utilize zircons as records of the Eoarchean to Hadean geomagnetic field we must investigate whether they have experienced reheating after crystallization but prior to incorporation into the conglomerate. Tarduno et al. (1) approached this in two ways. First, U-Pb data were reviewed for evidence of Pb loss that might have accompanied hypothetical reheating. Second, nonsystematic changes in Pb abundance during sensitive high-resolution ion microprobe (SHRIMP) analyses, seen in studies of other zircons that have experienced amphibolite to granulite grade metamorphism and thought to be a signal of Pb redistribution (46), were investigated. These checks were incorporated into selection criteria (1). We note that another critique claimed that instrumentation bias would exclude detection of nonsystematic changes (47). But this criticism omitted key information: Data collection on JH zircons (1) utilized the same SHRIMP instrument for which nonsystematic changes had been documented for zircons that had experienced high-grade metamorphism. While it is well known that SHRIMP cannot distinguish Pb abundance on an atomic scale, we show below that it has recorded nonsystematic changes in Pb in some JH zircons which we deselect in our analyses.

A different approach to the problem has been developed by Trail et al. (48) who suggested that Li zoning could be used as a qualitative indicator of the maximum postcrystallization temperature experienced by a zircon. This has in turn been

challenged by Tang et al. (49) who focus on limitations of Li diffusion by charge coupling with rare earth elements (REE) and Y in zircons from a granulite grade xenolith (Tanzania), tonalite–trondhjemite–granodiorites, and a sanukitoid (Superior Province, Canada). However, Trail et al. (48) clearly document Li diffusion independent of REE's mobility (50), indicating that the method is applicable to some zircons. We proceed with the method with the caveat that additional studies are needed to study charge-coupling–limited processes in JH and other zircons.

We collected ^{7}Li data using Cameca IMS 7f secondary-ion mass spectrometry (SIMA) at the University of Manitoba. For JH zircon Z565-12 [4.2 Ga (1)], the minimum measured Li bandwith is ~3.3 μm (Fig. 6 *A*–*C*) which corresponds to an estimated peak metamorphic heating of 475 °C (48) (*Materials and Methods* and *SI Appendix*, Table S3). Peak temperature predictions using the slope between Li zoning bands yield consistent peak temperature values (Fig. 6*D*).

Similar temperature estimates are available from other Hadean zircons studied by Tarduno et al. (1) that lack evidence for predepositional Pb loss (*SI Appendix*, Figs. S7 and S8 and Table S3). However, we note that one Hadean grain highlighted by Tarduno et al. (1) with Pb loss of ambiguous age yields much less-well defined bands which may indicate enhanced Li diffusion; the estimated peak temperature is ~560 °C (*SI Appendix*, Fig. S9 and Table S3).

Thus, notwithstanding the aforementioned caveats on the method, the Hadean grains passing all selection criteria (1) yield peak reheating estimates that are remarkably similar to the peak postdepositional greenschist metamorphic event (18, 19), supporting the conclusion that select JH zircons were not reheated after crystallization to temperatures that would reset their high unblocking temperature magnetizations (1, 21, 23, 24, 28, 29, 48).

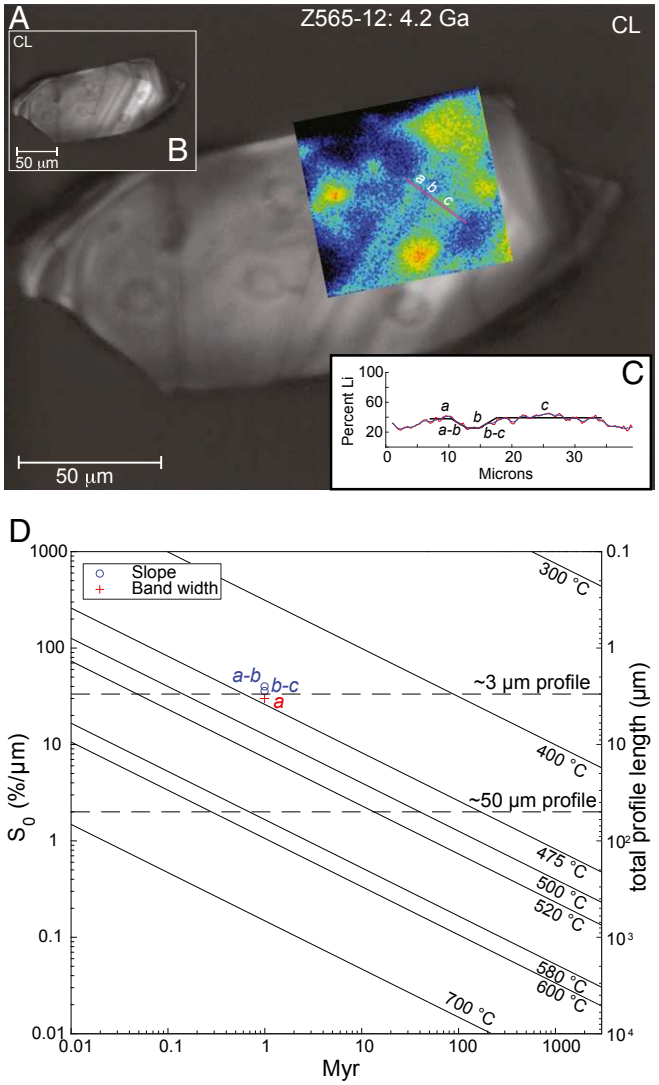

Fig. 6. Lithium profiling in magnetized 4.2-Ga Jack Hills zircon. (*A*) Cathodoluminescence (CL) image of zircon yielding a 12.8-μT paleofield (1). Dark pits are age analysis spots. (*B*) CL image with superimposed ^{7}Li image. (*C*) ^{7}Li image, transect, and band widths and slopes used to assess maximum heating since formation using geospeedometry (48) (*Materials and Methods*). (*D*) Band width and slope values for 4.2-Ga zircon and estimates for other Hadean grains (*SI Appendix*, Figs. S5 and S6) are consistent with reheating no greater than that associated with Jack Hills greenschist metamorphism.

New Data Defining a Paleoarchean–Hadean Geodynamo

Having provided further evidence for minimal reheating prior to conglomerate deposition, we now follow the methods and selection criteria of Tarduno et al. (1) to further evaluate JH zircons. We analyze zircons from the same host rock on which the prior microconglomerate and inverse microconglomerate tests have been conducted. We evaluate paleointensity using both full Thellier–Coe analyses and determinations at 565 °C with multidomain tail checks (*Materials and Methods*). However, we address one final critique claiming that magnetite detected by unblocking data (1) is not intrinsic but created during heating (31). This criticism neglects the salient features of the experimental protocol, magnetic mineral physics, and data. The use of a CO_2 laser heats over such short timescales (i.e., 90 s) that alteration is limited (15). Conjectural magnetite formation requires a precursor, and the only potential source would be ferric iron seen in JH zircons compromised by metamictization (31) (*SI Appendix*). But an ~230 times increase in room temperature saturation magnetization (M_s) accompanies the conversion of a hypothetical ferric parent phase (e.g., hematite, M_s of 0.4 A m^2/kg) to daughter magnetite (M_s of ~92 A m^2/kg). During the first applied-field step of the 565 °C paleointensity determinations, a huge increase in intensity is expected, but absent in the data (*SI Appendix*, Figs. S10 and S11). The largest increase observed is only 0.007% of that predicted and attributable to the removal of complex low-temperature overprints, with directions partially opposed to the characteristic high-temperature remanence, masking its intensity. Thus, the claim that magnetite produced by heating is responsible for the paleointensity signal is unfounded.

Data from one full Thellier–Coe analysis and twenty-three 565 °C analyses met selection criteria (*SI Appendix*, Tables S4 and S5 and Fig. 7*A*). SHRIMP geochronological analyses yield ^{207}Pb/^{206}Pb ages between ~3.35 and 4.13 Ga for these samples (*SI Appendix*, Table S6). These select data lack evidence of disturbance, beyond that associated with the ~2.65-Ga metamorphic event, and as well lack the nonsystematic changes in Pb counts that we use as part of our selection criteria (1). We note, however, that some rejected zircons have characteristics that may mark reheating after formation but prior to deposition. Nonsystematic changes in Pb are observed in these SHRIMP data as is Pb-Pb age evidence for one or more reheating episodes (Fig. 7*B*). The latter includes an event at ~3.4 Ga, noted in prior studies (51), in a zircon with an exceptionally old core (~4.3 Ga, zircon NZ_S59).

All of the new paleointensities are above the geodynamo presence threshold (1, 2). These new data, combined with those of the first zircon paleointensity analyses, yield some interesting features (Fig. 8). Fifty percent of the data have ages within

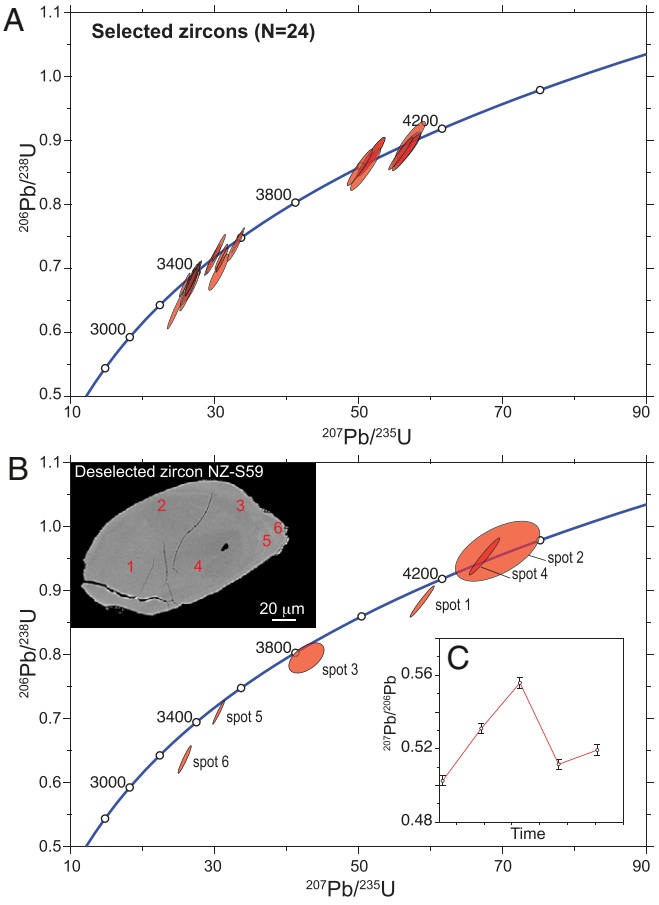

Fig. 7. New geochronological analyses on Jack Hills zircons. (*A*) Concordia diagram showing SHRIMP geochronological data for samples meeting selection criteria (*SI Appendix*, Table S6). (*B*) Zircon NZ-S59 has an exceptionally old core (4.3 Ga, spot 2, *Inset*) but the data fail criteria established by Tarduno et al. (1). The data show evidence of multiple potential reheating events. Moreover, the data in *B* show nonsystematic changes with time (spot 2, *C*).

50 My of 3.4 Ga, further highlighting the importance of this magmatism recorded at the Discovery Site. The mean paleointensity of this age group (n = 34) is 10.8 ± 6.3 μT. If we exclude the one zircon with Pb loss and Li diffusion characteristics that could reflect reheating, there are three Hadean paleointensity values between 4.02 and 4.13 Ga (24.5 ± 6.5 μT) that are more than two times greater than the 3.4 Ga value. This pattern yields further support for the primary nature of the remanence. Specifically, the 3.4-Ga data cluster clearly defines this age as the most important magmatic event that could potentially overprint our Discovery Site zircons prior to deposition. If the 4.02- to 4.13-Ga Hadean zircons had been magnetically reset, their paleointensity values should be lower than observed. In addition, conjectural secondary magnetite, as discussed earlier, would further bias the field to low, not high, values (*SI Appendix*). This hypothetical underestimate has its origin in several complementary processes: Chemical remanent magnetizations carried by secondary grains are inefficient relative to TRMs, and select areas of conjectural secondary magnetic grain growth within a zircon are unlikely to hold remanences on billion-year timescales because of Maxwell–Boltzmann statistics. Even if enough secondary grains to hold a remanence formed, the vector addition of such a magnetization with the primary direction would result in an overall lower apparent NRM intensity unless the primary and secondary directions were exactly aligned. However, all secondary grains will tend to acquire a uniform laboratory TRM. This strong TRM, relative to the lowered NRM, results in artificially low paleointensities, inconsistent with observations (Fig. 8).

The emerging pattern of paleointensity values is intriguing. Because each zircon paleointensity value averages at least several tens of thousands of years (1), the trends are unlikely to represent only an intrinsic variability similar to that of the modern dynamo (although a different dynamo variability cannot be excluded with the small number of paleointensity determinations currently available). The oldest paleointensity value at 4.2 Ga is based on a single value, but this grain has both Pb-Pb and Li characteristics supporting a primary recording. Core cooling sufficient to drive convection at 4.2 Ga may have been dominated by a heat pipe mode of heat transport through the mantle (52). One hundred million years later, field values are approximately two times higher. In the Eoarchean, the field drops by a factor of ∼2. The available data suggest only minor variations henceforward, until ∼3.2 Ga. Olson and Christensen (53) used the results of dynamo numerical simulations to suggest that dipole moment (M_D) increases with convective buoyancy flux (F) as $M_D \sim F^{1/3}$. Thus, the factor of 2 change in field strength in the late Hadean suggests a factor of 8 change in cooling across the core mantle boundary. This change seems unrealistically large for the Hadean core given the likelihood of a basal magma ocean (54). The rapid change in Hadean field strengths could instead reflect the onset of MgO exsolution, which is expected to provide a sudden boost to the dynamo (55, 56). The pattern is consistent with a core that is initially undersaturated in MgO, with precipitation commencing after several hundred million years of cooling. Temporal changes in core SiO_2 precipitation (57) might also be recorded by these data. The drop in field strength in the Eoarchean correlates in time with the Late Heavy Bombardment (LHB), which is opposite to the Hadean field strength–impact flux relationship proposed by O'Neill et al. (58). Instead, the potential drop in field intensity may reflect the development of core–mantle boundary heterogeneity associated with cooling of a basal magma ocean. This could have driven core-mantle boundary (CMB) heat flow, the core velocity field, and the resulting magnetic field to smaller length scales, ultimately resulting in a lower net surface magnetic-field strength. Alternatively, if final solidification of a basal magma ocean occurred in the Eoarchean, this would likely result in a strong drop in CMB heat flow and an attendant drop in magnetic-field intensity. While the Hadean/Eoarchean history is tentative because of the small number of acceptable paleointensity analyses, the available data nevertheless highlight the potential of zircon magnetizations to track evolution of fundamental core processes.

Materials and Methods

Paleomagnetism and Paleointensity. Procedures follow those outlined in Tarduno et al. (1) and Cottrell et al. (21). Below, we briefly review salient points of these techniques and include new methods applied at AIST. For the preparation of oriented zircons, the geographic orientation line of the field-collected hand sample was transcribed onto the cut billet from which the 300- to 500-μm thick sections were derived. All documentation photographs were taken relative to the projection of the down dip azimuth plane (vertical). Zircons in quartz were isolated from the same sections that were studied by Cottrell et al. (21) for paleomagnetic directions held by fuchsite. Excess material was etched away using a sodium silicate–alumina powder to leave a small pillar of zircon in quartz on the oriented microscope slide. The slide was then trimmed to an area ∼2 mm × 2 mm in size with the pillar of zircon in quartz centered on the subslide. To study the TRM imparted at 565 °C on zircon in quartz versus quartz alone, a sample originally measured by Tarduno et al. (1) was removed from the microscope subslide with the use of acetone and distilled water in an oscillating water bath. The sample was then remounted in a 27-mm × 27-mm × 2-mm fused quartz slide that had been precision drilled with a diamond tip to produce a 600-μm diameter well, ∼500 μm deep. Both quartz and zircon in quartz from the same slide (slide1-z1) and quartz of approximately

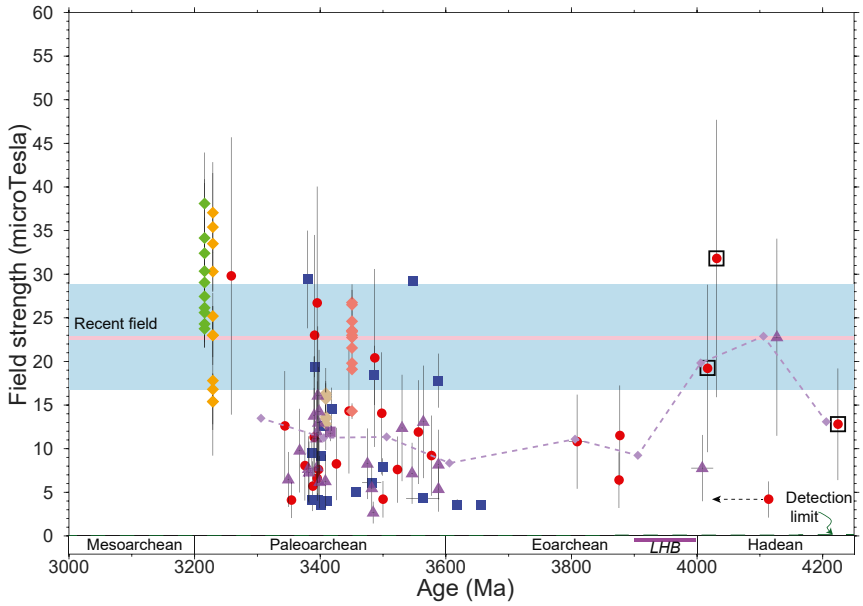

Fig. 8. Paleointensity vs. time from Jack Hills zircons. Zircon paleointensity results: blue boxes, Thellier–Coe paleointensity results from Tarduno et al. (1); red circles, 565 °C paleointensity determinations from Tarduno et al. (1); purple box, Thellier–Coe paleointensity result (this study); purple triangles, 565 °C paleointensity determinations (this study). Thellier–Coe paleointensity uncertainties are plotted at 1σ; uncertainties for 565 °C paleointensity determinations are a factor of two bounds (1). Age uncertainties are plotted at 1σ. Large open black boxes: ^{7}Li profiling geospeedometry constraints (54) indicating maximum temperature <475 °C. Dashed line with arrow: ^{7}Li profiling highlighting potential for magnetic resetting. Purple diamonds and line: 100-My running average of zircon paleointensity results excluding potentially reset value. Recent field: Pink solid line is mean equatorial field value and SD (blue shaded region) from a bootstrap resampling of data from the past 800,000 y (1). Single silicate crystal results (equatorial equivalent values assuming a dipole-dominated field) from prior studies of extant rocks are shown by green (15), yellow (15), tan (5), and pink (5) diamonds. LHB: Late Heavy Bombardment. All data are above threshold for geomagnetic field presence (dashed green line) based on external field imparted by the solar wind from Tarduno et al. (2).

the same dimensions were then given a TRM with a 40-W Synrad CO_2 laser at AIST and transferred, using Mu-metal shields, to the AIST SSM for measurement. SSM measurements (32) were conducted in a scanning area of 6 mm × 6 mm at 50 μm grid spacing. The distance of the sensor to the surface of a slide is calculated as ∼240 μm based on a precision line current scan. The simplified 565 °C paleointensity approach (1) was applied to limit the effects of laboratory-induced alteration. After measurement of the NRM, the sample was gradually heated in field-free space; this was accomplished by holding the temperature for 1 min at 100 °C temperature increments to 500 °C. Thereafter, the temperature was increased to 565 °C for an additional 1 min and then allowed to cool, for 3 to 5 min. A second heating to 565 °C was performed next in the presence of a field. Finally, a multidomain check was performed by reheating the sample to 565 °C in the absence of a field. Analyses in ref. 1 indicate that paleointensity values obtained at 565 °C are within a factor of 2 of full Thellier–Coe results.

Optical Microscopy and MOKE. Optical microscopy studies (University of Rochester) used a Nikon Eclipse LV100POL microscope with both transmitted and reflected light capabilities, a maximum 1,000× magnification, and a Spot Insight 4MP CCD color digital camera assembly. MOKE analyses were performed at the Naval Research Laboratories. Grains were mounted on epoxy stubs and polished (first with alumina to 0.5 μm followed by 0.05 μm colloidal silica) to expose the grain interiors. The instrument employed (Quantum Designs NanoMOKE3) is capable of detecting micrometer to submicrometer magnetic features at depths on the order of 1 to 10 μm beneath the polished surface. Samples were exposed to a magnetic field (∼500 mT) and imaged using both polar (field applied normal to grain surface) and longitudinal (field applied parallel to grain surface) modes. Reflected laser light and Kerr effect images were collected simultaneously, allowing for the discrimination between optical and magneto-optical features.

SEM, FIB, and TEM. A FIB (equipped in an FEI Strata 400 located at Cornell Center for Materials Research) was used to mill a trench in zircon JHZ5-4X-7 to examine the source of a strong MOKE signal by preparing a lift-out lamella (59, 60). A platinum layer was deposited prior to FIB milling to protect the grain surface above the target region from FIB damage. An ∼1-μm thick lamella containing a multipart inclusion was removed from the zircon matrix and mounted to a TEM copper grid. Due to the fragility of the multipart inclusion, the sample lamella was not further thinned to electron transparency thicknesses (<100 nm), precluding further TEM study of the sample. Nevertheless, the prepared lamella allowed for improved SEM and EDS characterization by removing the contribution from the surrounding zircon matrix which typically contributes to the overall signal in other analyses. SEM and FIB analyses were also conducted at the University of Rochester using a Zeiss Auriga SEM. TEMs were conducted at the University of Rochester using an FEI Tecnai F20 G2 S/TEM (field emission, 200 kV) equipped with an EDAX energy-dispersive X-ray spectrometer.

Li Analyses. Cameca IMS 7f Li maps show narrow bands corresponding to oscillatory and/or sectoral zonation. Profiles ∼1 μm wide were selected for analysis. Along-profile Li values were smoothed with an ∼1-μm sliding-window filter and used to estimate band widths and slopes. Assigned temperatures assume an ∼1-My duration of orogenic heating. The more diffuse bands in one zircon (Z565-5) were analyzed to obtain a maximum temperature estimate as follows: Li profiles of 20 approximately uniformly spaced tracks were considered. A mean profile, 1σ uncertainty, and smoothed mean profile were calculated. From this smoothed mean profile, peaks and troughs of Li were assigned and slopes calculated.

Geochronology. Analytical procedures are detailed in the materials and methods section of Tarduno et al. (1) except where noted in *SI Appendix*, Table S6.

Data Availability. Magnetic datasets generated during and/or analyzed in this study are available in the MagIC repository, http://earthref.org/MagIC/16680.

ACKNOWLEDGMENTS. This work was supported by National Science Foundation (NSF) Grants EAR1520681 and EAR1656348 and a Japan Society for the Promotion of Science (JSPS) fellowship (to J.A.T.). O.v.'t.E. acknowledges support from core programs at the Naval Research Laboratory. We acknowledge help from Gerald Kloc in specimen preparation, B. L. McIntyre

and R. Wiegandt on electron microscopy analyses, T. Pestaj in the SHRIMP laboratory, and A. Katayama on AIST SSM measurements. We thank the anonymous reviewers for helpful comments. This work made use of the Cornell Center for Materials Research Shared Facilities which are supported through the NSF Materials Research Science and Engineering Centers (MRSEC) program (DMR-1719875).

1. J. A. Tarduno, R. D. Cottrell, W. J. Davis, F. Nimmo, R. K. Bono, A Hadean to Paleoarchean geodynamo recorded by single zircon crystals. *Science* **349**, 521–524 (2015).
2. J. A. Tarduno, E. G. Blackman, E. E. Mamajek, Detecting the oldest geodynamo and attendant shielding from the solar wind: Implications for habitability. *Phys. Earth Planet. Inter.* **233**, 68–87 (2014).
3. R. K. Bono, J. A. Tarduno, F. Nimmo, R. D. Cottrell, Young inner core inferred from Ediacaran ultra-low geomagnetic field intensity. *Nat. Geosci.* **12**, 143–147 (2019).
4. P. Driscoll, Geodynamo recharged. *Nat. Geosci.* **12**, 83–84 (2019).
5. J. A. Tarduno *et al.*, Geodynamo, solar wind and magnetopause 3.45 billion years ago. *Science* **327**, 1238–1240 (2010).
6. Y. Usui, J. A. Tarduno, M. K. Watkeys, A. Hofmann, R. D. Cottrell, Evidence for a 3.45-billion-year-old magnetic remanence: Hints of an ancient geodynamo from conglomerates of South Africa. *Geochem. Geophys. Geosyst.* **10**, Q09Z07 (2009).
7. A. J. Biggin *et al.*, Palaeomagnetism of Archaean rocks of the Onverwacht Group, Barberton Greenstone Belt (southern Africa): Evidence for a stable and potentially reversing geomagnetic field at ca. 3.5 Ga. *Earth Planet. Sci. Lett.* **302**, 314–328 (2011).
8. J. A. Tarduno, Geodynamo history preserved in single silicate crystals: Origins and long-term mantle control. *Elements* **5**, 217–222 (2009).
9. J. A. Tarduno, R. D. Cottrell, A. V. Smirnov, The paleomagnetism of single silicate crystals: Recording geomagnetic field strength during mixed polarity intervals, superchrons, and inner core growth. *Rev. Geophys.* **44**, RG1002 (2006).
10. T. Berndt, A. R. Muxworthy, K. Fabian, Does size matter? Statistical limits of paleomagnetic field reconstruction from small rock specimens. *J. Geophys. Res.* **121**, 15–26 (2016).
11. G. Pullaiah, E. Irving, K. L. Buchan, D. J. Dunlop, Magnetization changes caused by burial and uplift. *Earth Planet. Sci. Lett.* **28**, 133–143 (1975).
12. D. J. Dunlop, Ö. Özdemir, *Rock Magnetism, Fundamentals and Frontiers* (Cambridge University Press, New York, NY, 1997).
13. T. P. Almeida *et al.*, Direct visualization of the thermomagnetic behavior of pseudo-single-domain magnetite particles. *Sci. Adv.* **2**, e1501801 (2016).
14. S. A. Wilde, J. W. Valley, W. H. Peck, C. M. Graham, Evidence from detrital zircons for the existence of continental crust and oceans on the Earth 4.4 Gyr ago. *Nature* **409**, 175–178 (2001).
15. J. A. Tarduno, R. D. Cottrell, M. K. Watkeys, D. Bauch, Geomagnetic field strength 3.2 billion years ago recorded by single silicate crystals. *Nature* **446**, 657–660 (2007).
16. M. Barboni *et al.*, Early formation of the moon 4.51 billion years ago. *Sci. Adv.* **3**, e1602365 (2017).
17. M. Sato, Rock-magnetic properties of single zircon crystals sampled from the Tanzawa tonalitic pluton, central Japan. *Earth Planets Space* **67**, 150 (2015).
18. B. Rasmussen, I. R. Fletcher, J. R. Muhling, S. A. Wilde, In situ U-Th-Pb geochronology of monazite and xenotime from the Jack Hills belt: Implications for the age of deposition and metamorphism of Hadean zircons. *Precambrian Res.* **180**, 26–46 (2010).
19. B. Rasmussen, I. R. Fletcher, J. R. Muhling, C. J. Gregory, S. A. Wilde, Metamorphic replacement of mineral inclusions in detrital zircon from Jack Hills, Australia: Implications for the Hadean earth. *Geology* **39**, 1143–1146 (2011).
20. G. S. Watson, A test for randomness of directions. *Geophys. J. Int.* **7**, 160–161 (1956).
21. R. D. Cottrell, J. A. Tarduno, R. K. Bono, M. S. Dare, G. Mitra, The inverse microconglomerate test: Further evidence for the preservation of Hadean magnetizations in metasediments of the Jack Hills, western Australia. *Geophys. Res. Lett.* **43**, 4215–4220 (2016).
22. B. P. Weiss *et al.*, Reply to comment on "Pervasive remagnetization of detrital zircon host rocks in the Jack Hills, Western Australia and implications for records of the early dynamo". *Earth Planet. Sci. Lett.* **450**, 409–412 (2016).
23. M. S. Dare *et al.*, Detrital magnetite and chromite in Jack Hills quartzite cobbles: Further evidence for the preservation of primary magnetizations and new insights into sediment provenance. *Earth Planet. Sci. Lett.* **451**, 298–314 (2016).
24. R. K. Bono, J. A. Tarduno, M. S. Dare, G. Mitra, R. D. Cottrell, Cluster analysis on a sphere: Application to magnetizations from metasediments of the Jack Hills, western Australia. *Earth Planet. Sci. Lett.* **484**, 67–80 (2018).
25. J. A. Tarduno, R. D. Cottrell, Signals from the ancient geodynamo: A paleomagnetic field test on the Jack Hills metaconglomerate. *Earth Planet. Sci. Lett.* **367**, 123–132 (2013).
26. B. P. Weiss *et al.*, Pervasive remagnetization of detrital zircon host rocks in the Jack Hills, Western Australia and implications for records of the early geodynamo. *Earth Planet. Sci. Lett.* **430**, 115–128 (2015).
27. W. Huang, J. A. Tarduno, R. D. Cottrell, R. K. Bono, E. R. Thern, Unraveling Archean magnetic histories by a comparison of whole rock and single crystal analyses of granites from Western Australia. Abstract GP21B-0651,American Geophysical Union 2018 Fall Meeting, 10–14 December, Washington, DC.
28. R. K. Bono, J. A. Tarduno, R. D. Cottrell, Comment on: Pervasive remagnetization of detrital zircon host rocks in the Jack Hills, Western Australia and implications for records of the early dynamo, by Weiss et al. (2015). *Earth Planet. Sci. Lett.* **450**, 406–408 (2016).
29. R. K. Bono, J. A. Tarduno, R. D. Cottrell, Primary pseudo-single and single-domain magnetite inclusions in quartzite cobbles of the Jack Hills (western Australia): Implications for the Hadean geodynamo. *Geophys. J. Int.* **216**, 598–608 (2019).
30. R. T. Pidgeon, S. A. Wilde, The interpretation of complex zircon U-Pb systens in Archaean granitoids and gneisses from the Jack Hills, narryer gneiss terrane, western Australia. *Precambrian Res.* **91**, 309–332 (1998).
31. B. P. Weiss *et al.*, Secondary magnetic inclusions in detrital zircons from the Jack Hills, Western Australia, and implications for the origin of the geodynamo. *Geology* **46**, 427–430 (2018).
32. H. Oda *et al.*, Scanning SQUID microscope system for geological samples: System integration and initial evaluation. *Earth Planets Space* **68**, 179 (2016).
33. D. Heslop, A. P. Roberts, A Bayesian approach to the paleomagnetic conglomerate test. *J. Geophys. Res.* **123**, 1132–1142 (2018).
34. R. K. Bono, J. A. Tarduno, R. D. Cottrell, M. S. Dare, The paleomagnetic record of Eoarchean to Hadean zircons: Magnetic hysteresis, imaging magnetic sources, micromagnetic modeling and constraining post-formation heating. Abstract GP22A-07, American Geophysical Union 2016 Fall Meeting, 12–16 December, San Francisco, CA.
35. J. A. Tarduno *et al.*, Earth's paleomagnetosphere and planetary habitability. Abstract P53E-2231, American Geophysical Union 2017 Fall Meeting, 11–15 December, New Orleans, LA .
36. G. Mitra, Ductile deformation zones and mylonites: The mechanical processes involved in the deformation of crystalline basement rocks. *Am. J. Sci.* **278**, 1057–1084 (1978).
37. D. D. Pollard, A. Aydin, Progress in understanding jointing over the past century. *Geol. Soc. Am. Bull.* **100**, 1181–1204 (1988).
38. S. M. Reddy, N. E. Timms, W. Pantleon, P. Trimby, Quantitative characterization of plastic deformation of zircon and geological implications. *Contrib. Mineral. Petrol.* **153**, 625–645 (2007).
39. J. D. Eshelby, F. C. Frank, F. R. N. Nabarro, The equilibrium of linear arrays of dislocations. *Philos. Mag.* **42**, 351–364 (1961).
40. Tang *et al.*, Secondary magnetite in ancient zircon precludes analysis of a Hadean geodynamo. *Proc. Natl. Acad. Sci. U.S.A.* **116**, 407–412 (2018).
41. M. Takehara, K. Horie, T. Hokada, S. Kiyokawa, New insight into disturbance of U-Pb and trace-element systems in hydrothermally altered zircon via SHRIMP analyses of zircon from the Duluth gabbro. *Chem. Geol.* **484**, 168–178 (2018).
42. J. M. Feinberg, G. R. Scott, P. R. Renne, H.-R. Wenk, Exsolved magnetite inclusions in silicates: Features determining their remanence behavior. *Geology* **33**, 513–516 (2005).
43. R. Symonds, Scanning electron microscope observations of sublimates from Merapi Volcano, Indonesia. *Geochem. J.* **26**, 337–350 (1993).
44. J. P. Bradley, H. Y. McSween Jr., R. P. Harvey, Epitaxial growth of nanophase magnetite in Martian meteorite Allan Hills 84001: Implications for biogenic mineralization. *Meteorit. Planet. Sci.* **33**, 765–773 (1998).
45. P. N. Argyres, Theory of the Faraday and Kerr effects in ferromagnetics. *Phys. Rev.* **97**, 334–345 (1955).
46. W. J. Davis, N. Rayner, T. Pestaj, "When good zircons go bad-redistribution of radiogenic Pb in granulite grade zircon, snowbird tectonic zone, Canada" in *Abstract Volume, 4th International SHRIMP Workshop, Saint Petersburg, Russia*, O. Petrov, S. Shevchenko, S. Sergeev, L. Mordberg, Eds. (VSEGEI Press, St. Petersburg, Russia, 2008), pp. 42–44.
47. T. M. Harrison, E. A. Bell, P. Boehnke, Hadean zircon petrochronology. *Rev. Mineral. Geochem.* **83**, 329–363 (2017).
48. D. Trail *et al.*, Li zoning in zircon as a potential geospeedometer and peak temperature indicator. *Contrib. Mineral. Petrol.* **171**, 25 (2016).
49. M. Tang, R. L. Rudnick, W. F. McDonough, M. Bose, Y. Goreva, Multi-mode Li diffusion in natural zircons: Evidence for diffusion in the presence of step-function concentration boundaries. *Earth Planet. Sci. Lett.* **474**, 110–119 (2017).
50. J. T. Sliwinski *et al.*, Controls on lithium concentration and diffusion in zircon. *Chem. Geol.* **501**, 1–11 (2018).
51. J. W. Valley *et al.*, Hadean age for a post-magma-ocean zircon confirmed by atom-probe tomography. *Nat. Geosci.* **7**, 219–223 (2014).
52. W. B. Moore, A. A. G. Webb, Heat-pipe Earth. *Nature* **501**, 501–505 (2013).
53. P. Olson, U. R. Christensen, Dipole moment scaling for convection-driven planetary dynamos. *Earth Planet. Sci. Lett.* **250**, 561–571 (2006).
54. S. Labrosse, J. W. Hernlund, N. Coltice, A crystallizing dense magma ocean at the base of the Earth's mantle. *Nature* **450**, 866–869 (2007).
55. J. G. O'Rourke, D. J. Stevenson, Powering Earth's dynamo with magnesium precipitation from the core. *Nature* **529**, 387–389 (2016).
56. J. Badro, J. Siebert, F. Nimmo, An early geodynamo driven by exsolution of mantle components from Earth's core. *Nature* **536**, 326–328 (2016).
57. K. Hirose *et al.*, Crystallization of silicon dioxide and compositional evolution of the Earth's core. *Nature* **543**, 99–102 (2017).
58. C. O'Neill, S. Marchi, S. Zhang, W. Bottke, Impact-driven subduction on the Hadean Earth. *Nat. Geosci.* **10**, 793–797 (2017).
59. L. A. Giannuzzi, F. A. Stevie, A review of focused ion beam milling techniques for TEM specimen preparation. *Micron* **30**, 197–204 (1999).
60. J. Mayer, L. A. Giannuzzi, T. Kamino, J. Michael, TEM sample preparation and FIB-induced damage. *MRS Bull.* **32**, 400–407 (2007).